DE GRUYTER Z. Kristallogr. 2019; 234(9): 587–593

Carsten Paulmann, Peter Zietlow, Catherine McCammon, Ekhard K.H. Salje and Ulrich Bismayer*

Annealing of metamict gadolinite-(Y): X-ray diffraction, Raman, IR, and Mössbauer spectroscopy

https://doi.org/10.1515/zkri-2019-0014
Received March 13, 2019; accepted May 27, 2019; published online June 13, 2019

Abstract: Radiation induced disorder in gadolinite that led to metamictization with an upper degree of amorphization of 18% was thermally annealed between room temperature and 1273 K. The degree of annealing was calibrated using the anti-symmetric Si–O–Si Raman-active stretching mode near 902 cm^{-1}. Annealing increased with increasing temperature with a rapid critical recrystallization at ca. 943 K. This annealing on a short length scale was then complemented by investigations of long-range ordering seen by X-ray diffraction. The same critical temperature was found, and in addition further increase of long-range order extended to 1073 K. Metamict gadolinite contains only Fe^{2+} within experimental uncertainty.

Keywords: infrared; metamict gadolinite-(Y); Mössbauer spectroscopy; Raman; X-ray powder diffraction.

Introduction

Metamict minerals show radiation-induced structural disorder caused by the decay of radionuclides that are incorporated in their structure or in the neighbouring minerals. For more than half a century, experimental and theoretical studies have been undertaken in order to better understand the metamict state and important characteristics such as the partially or heavily damaged crystal structure compared to the long-range ordered crystalline state. It had been shown that thermal annealing often leads to the recovery of the crystalline order depending on the level of the structural damage [1, 2].

The mineral gadolinite was named in the nineteenth century after the Finnish scientist Johan Gadolin. With the increasing use of rare earth elements in electronic devices, gadolinite is considered to be an important source of Y, Ce and Gd. Its typical chemical formula is $(REE)_2FeBe_2O_2(SiO_4)_2$ where REE=Ce, Y and contains minor amounts of other lanthanides. In the metamict state it may also contain minor amounts of OH-groups. The undamaged crystal structure of the yttrium-containing gadolinite was studied by Pavlov and Belov [3] and Miyawaki et al. [4] who determined the space group as $P2_1/a$ with lattice parameters $a=10.000(2)$ Å, $b=7.565(2)$ Å, $c=4.768(1)$ Å, $\beta=90.31(2)^o$ and $V=360.7(1)$ Å^3. The structure is displayed in Figure 1 approximately along a.

Natural gadolinite shows different stages of metamictization related to the varying proportion of radionuclides (like U and Th) on the REE site that leads to self-radiation, which causes alpha-recoil damage of the crystalline order. From other metamict minerals it is known that thermal treatment leads to recrystallization that restores medium and long-range order [5–13]. The extent of recrystallization depends on the mineral structure and the initial degree of amorphization [14–16]. Recrystallization of the metamict state in zircon was shown not to proceed by simple growth of the crystalline zircon structure inside an amorphous matrix but entails a number of metastable intermediate states. These states may survive for long times and can not all be characterized on a laboratory time scale. The recrystallization process also depends sensitively on the degree of metamictization where surviving undamaged grains play the role of nucleation centres which lead to recrystallization by front propagation, while more highly metamictized samples proceed by clouds of small nucleation centres [10, 11, 17].

In this work we study the recrystallization of metamict gadolinite using several experimental techniques to disentangle structural changes on different lengths scales. A sample of metamict gadolinite-(Y) with ca. 18%

***Corresponding author: Ulrich Bismayer,** Mineralogisch-Petrographisches Institut, Universität Hamburg, Grindelallee 48, 20146 Hamburg, Germany, E-mail: ubis@uni-hamburg.de
Carsten Paulmann and Peter Zietlow: Mineralogisch-Petrographisches Institut, Universität Hamburg, Grindelallee 48, 20146 Hamburg, Germany
Catherine McCammon: Bayerisches Geoinstitut, Universität Bayreuth, D-95440 Bayreuth, Germany
Ekhard K.H. Salje: Department of Earth Sciences, University of Cambridge, Downing street, Cambridge CB2 3EQ, UK

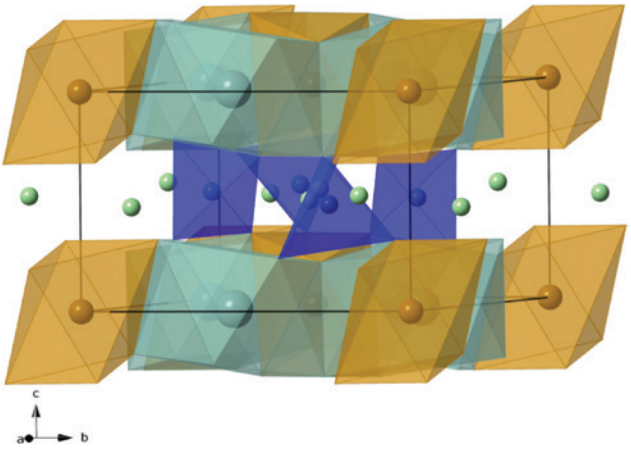

Fig. 1: Polyhedral model of gadolinite showing SiO_4-tetrahedra, with distorted Fe–O-octahedra, eight-fold coordinated REE polyhedra and Be positions (four-fold coordinated by O; tetrahedra not shown for clarity) in layers (atomic positions from [4]). Plotted using CrystalMaker Software, UK.

amorphous fraction was subjected to thermal annealing. The degree of metamictization after annealing experiments between room temperature and 1273 K was determined by X-ray diffraction, and Raman and IR spectroscopy, and compared with earlier studies [18–20]. Metamict minerals often contain Fe as impurity as a structural element. Amorphization can promote the formation of Fe^{2+} while, often, Fe^{3+} is found in recrystallized samples. A typical example is titanite where the transition Fe^{2+} to Fe^{3+} mirrors the recrystallization process [10–12]. The metamict sample of gadolinite contains only Fe^{2+} within experimental uncertainty which raises the question as to whether the transformation on annealing mirrors the recrystallization process or not via the valence state of Fe as has been observed in titanite.

Experimental

Gadolinite sample

The sample used in this study is a natural gadolinite-(Y) mineral from the collection at the Mineralogisches Museum of the University of Hamburg. Its origin is the Setesdal location in Central South Norway, an igneous province between Oslo and Stavanger. The geologic age of the area is ca. 600–800 Ma [21, 22] and no metamorphic heating episodes above ca. 500 K were found to have occurred based on fission track measurements on the associated mineral titanite. Scherer et al. [23] report the gadolinite U/Pb age of a pegmatite of the southern Setesdal area to be 910 ± 14 Ma. There is no age information of the sample available for this study and we estimate that the accumulated dose may range between 3.9 and 6.2 10^{18} α-decay events/g. Such values have been confirmed in other gadolinite-bearing pegmatites [20],

Tab. 1: Electron microprobe analysis result of metamict gadolinite-(Y), Setesdal, Norway.

Oxide	wt. (%)
Al_2O_3	0.00
SiO_2	22.99
FeO	11.24
Y_2O_3	29.06
ThO_2	0.19
UO_2	0.00
Ce_2O_3	1.99
Pr_2O_3	0.59
Nd_2O3	4.31
SmO	2.52
Gd_2O_3	4.21
Tb_2O_3	0.00
Dy_2O_3	3.11
Ho_2O_3	0.56
Er_2O_3	2.15
Yb_2O_3	2.53
La_2O_3	0.24
Eu_2O_3	0.00
MgO	0.96
MnO	0.20
Total	86.85

but even lower dose ranges have also been reported for gadolinite from Scandinavia [24].

The sample is homogeneously dark brown with glass-like surface appearance and no cleavage. The chemical composition was measured using an electron microprobe (Cameca Cambax microbeam SEM system), details are described by Beirau et al. [16]. The acceleration voltage was 15 kV, the sample current 40 nA and the beam diameter 30 µm. Table 1 shows the result of the analysis. The chemical composition agrees with Chukanov et al. [25]. We did not calculate an empirical formula of gadolinite-(Y) because of the unknown amount of OH-groups of our sample.

X-ray powder diffraction

Powder X-ray diffraction patterns were collected using a Stoe powder diffractometer with Bragg Bretano geometry and Cu–Kα_1 radiation with an asymmetric Ge 111 monochromator. Progressive annealing experiments in a Thermo-Scientific Laboratory Chamber Furnace K114 with temperature stability ±2 K for 15 min at each temperature step (RT, 673 K, 873 K, 1073 K and 1273 K) were performed before mounting the sample on the diffractometer. The diffraction patterns of gadolinite-(Y) at room temperature and after annealing are shown in Figure 2. The amorphous fraction was determined from the relation of the integrated intensity of the Bragg (121) reflection at 2-θ of 31.1° and the background intensity of the untreated natural metamict sample, a technique described previously [13, 26, 27].

The monoclinic space group is $P2_1/c$ (standard setting) with 17 reflections observable at room temperature. After annealing more reflections occurred and the refinement improved. The refined lattice parameters are summarized in Table 2.

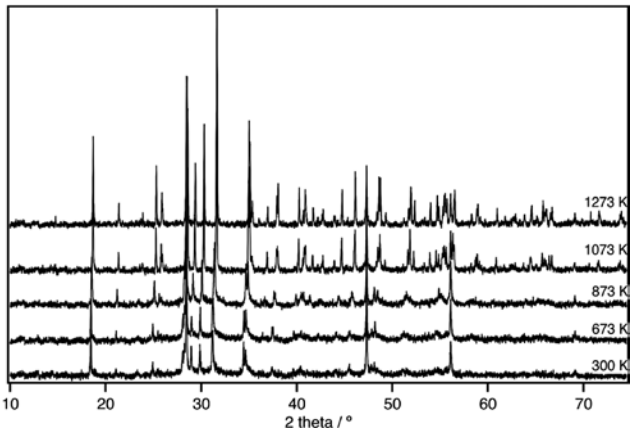

Fig. 2: Diffraction patterns of the gadolinite-(Y) sample at room-temperature (300 K) and after annealing for 15 min at the indicated temperatures.

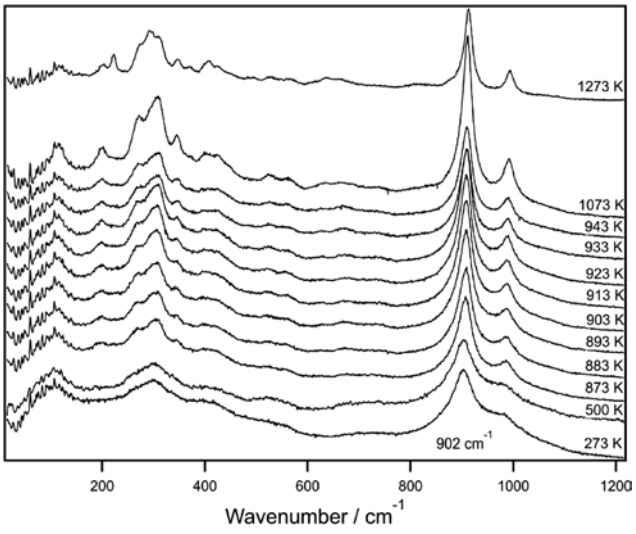

Fig. 3: Unpolarized Raman spectra of metamict gadolinite-(Y) of the untreated material at 273 K and the sample annealed for 15 min at the indicated temperatures.

Raman spectroscopy

Raman spectra of the gadolinite-(Y) sample were recorded at room temperature and after annealing. The measurements were performed on polished plane-parallel specimens using a Horiba Jobin-Yvon T64000 triple monochromator system operating in the subtractive regime and equipped with a liquid N_2-cooled charge-coupled device (CCD) detector and an Olympus BX41 microscope. Spectra were collected in backscattering geometry without analyzer of the scattered light, using the 514.5 nm line of an Ar^+-ion laser and a long-working distance objective with magnification 50×. The Raman spectroscopic system was calibrated with respect to the Si peak at 520.5 cm^{-1} with a precision of ±0.35 cm^{-1}. The measured spectra were corrected using the Bose-Einstein occupation factor and fitted by Voigt functions. The samples were annealed in a Linkam stage TS1200EV-10/5 with annealing times of 15 min per temperature step. Raman measurements were performed after cooling the annealed sample to room temperature. The unpolarized Raman spectra of the untreated metamict sample and the annealed samples are plotted in Figure 3.

FTIR spectroscopy

Infrared (IR) spectroscopy was performed using a Bruker FTIR Vertex 70 spectrometer equipped with a RT-DLaTGS detector. MIR-FIR powder infrared absorption spectra with instrumental resolution of 2 cm^{-1} were measured using KBr pellets. IR spectra of the metamict sample and the gadolinite-(Y) annealed for 15 min at 1073 K are shown in Figure 4.

Mössbauer spectroscopy

The natural gadolinite-(Y) sample was analysed using Mössbauer spectroscopy both before and after annealing. A doubly polished slice was prepared with dimensions of approximately 1 × 3 mm^2 and 150 µm thickness, giving a Mössbauer thickness of roughly 4 mg Fe/cm^2 which is close to the optimum thickness for this composition [28]. The slice was annealed in air in a Nabertherm N7/H box furnace equipped with a C20 program controller over a ramped profile with steps of 673, 873 and 1073 K for 15 min each, where the sample remained in the furnace from start to finish. Mössbauer spectra were collected at room temperature (293 K) over the same 1 mm diameter spot on the slice before and after annealing in transmission mode on a constant acceleration Mössbauer spectrometer with a nominal 0.37 GBq ^{57}Co point source (1 month old) in a 12 µm Rh matrix. The velocity scale was calibrated relative to 25 µm thick α-Fe foil using the positions certified for (former) National Bureau of Standards standard reference material no. 1541; line widths of 0.36 mm/s for

Tab. 2: Refined lattice parameters of gadolinite-(Y), monoclinic space group is $P2_1/c$ (standard setting).

T/K	No.	a/Å	b/Å	c/Å	β/°	V/Å³
RT	17	4.794 (62)	7.486 (42)	10.061 (105)	90.73 (76)	361.01 (4.12)
673	26	4.775 (14)	7.615 (15)	10.052 (33)	90.11 (24)	365.56 (1.19)
873	25	4.763 (9)	7.578 (9)	10.023 (25)	90.16 (15)	361.96 (0.68)
1073	32	4.740 (6)	7.555 (6)	9.978 (7)	90.32 (9)	357.39 (0.41)
1237	32	4.736 (6)	7.544 (6)	9.966 (8)	90.28 (9)	356.06 (0.45)

T, Annealing temperature in K; No., number of indexed reflections.

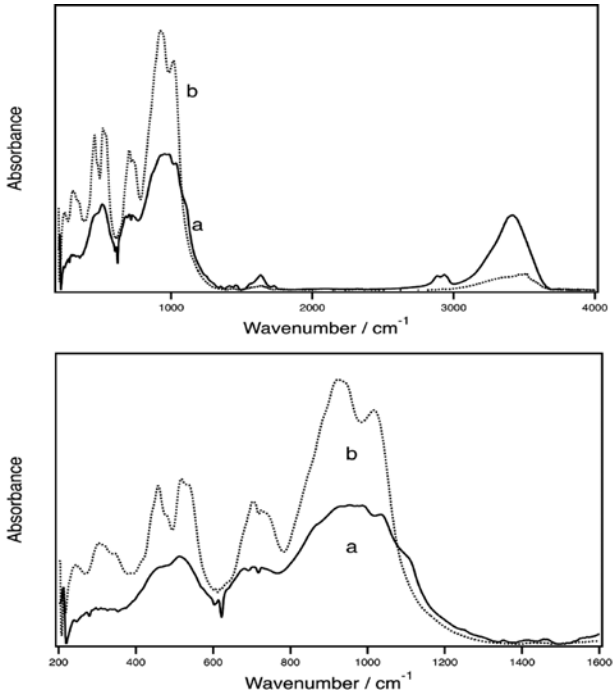

Fig. 4: IR spectrum of Setesdal gadolinite-(Y) of the untreated metamict sample (a) and the sample annealed for 15 min at 1073 K (b). The upper spectrum shows the entire range measured, while the lower spectrum shows an expanded region in the far infrared.

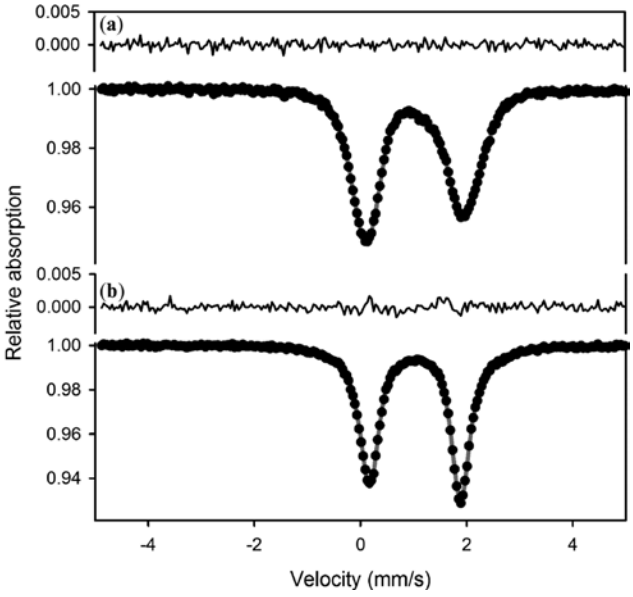

Fig. 5: Room temperature Mössbauer spectrum of natural Setesdal gadolinite-(Y) (a) and taken on the same slice after annealing (b). The spectra were fit to multiple pseudo-Voigt quadrupole doublets with weighted mean hyperfine parameters listed in Table 3. The fitted curve is shown in grey and the residual (difference between observed and calculated data) is shown above each spectrum.

Tab. 3: Hyperfine parameters derived from fits to Mössbauer spectra of gadolinite.

	<CS>	<QS>	<Γ>	A_{21}	D_{max}
	mm/s	mm/s	mm/s		
Natural	0.99 (3)	1.83 (5)	0.50 (7)	1.01 (1)	0.948
Annealed	1.03 (2)	1.80 (5)	0.24 (2)	1.11 (1)	0.929

<>, Weighted mean value; CS, centre shift relative to α-Fe; QS, quadrupole splitting; Γ, full width at half maximum; A_{21}, area ratio of high velocity component to low velocity component; D_{max}, maximum absorption.

the outer lines of α-Fe were obtained at room temperature. Each spectrum was collected for 1–2 days and was fitted using the program MossA [29].

The Mössbauer spectra appear similar to those reported by Malczewski [30] and Malczewski et al. [24] (Figure 5). Spectra were fit using multiple pseudo-Voigt quadrupole doublets to account for next-nearest neighbour effects. The weighted mean values of the hyperfine parameters are listed in Table 3. The spectrum of the natural sample is typical for Fe^{2+} in a phase that lacks a high degree of long-range order, where local site-to-site variations give rise to an asymmetrically broadened doublet (e.g. [31]). After annealing, the quadrupole doublet becomes narrower and symmetric in width, but develops an area asymmetry due to crystalline preferred orientation (e.g. [32]). The maximum absorption increases, presumably due to an increase in recoil-free fraction. There is no evidence for Fe^{3+} in either spectrum within the uncertainty of the data, where the detection limit for Fe^{3+} is estimated to be approximately 2% of total iron.

Results and discussion

Figure 2 shows the temperature evolution of the X-ray powder diffraction diagrams of the virgin metamict and the annealed gadolinite-(Y) sample. The diffuse background becomes weaker at higher temperatures and almost disappears above 873 K. Bragg reflections that exist in the untreated sample become stronger on annealing. Gradual shifts of the different peaks also appear, shown in Figure 6 for the (121) Bragg peak at a 2-θ value near 31°.

The amorphous fraction (X_{amorph}) of the untreated mineral was estimated from the broad amorphous background

$$X_{amorph} = \frac{I_{amorph}}{I_{amorph} + I_{Bragg}} \quad (1)$$

where I_{amorph} and I_{Bragg} are the integrated intensities of the amorphous background and the Bragg signal [13, 26, 27]. Based on the diffraction near the (121) reflection the resulting amorphous fraction is approximately 0.18 (with

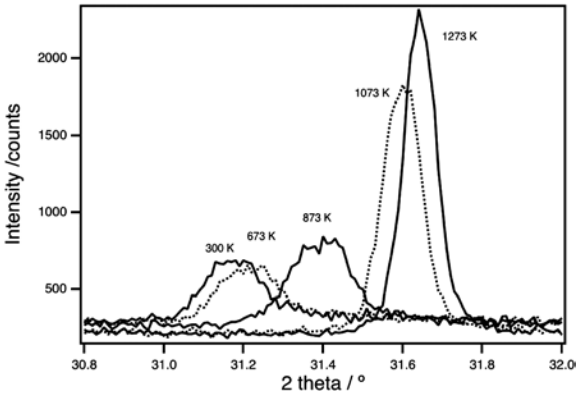

Fig. 6: Powder X-ray diffraction pattern near two-theta values of the (121) Bragg-peak at room temperature (300 K) and after annealing metamict gadolinite-(Y) at the indicated temperatures.

error on the order of 5%). The line width of the diffraction peaks decreases with increasing temperature. Annealing the metamict sample leads to the re-established long-range order of the sample as can be observed from this narrowing of the Bragg peaks, their shift and increased X-ray diffraction intensity (Figures 2 and 6).

The IR powder spectrum of gadolinite-(Y) (Figure 4) shows the effect of radiation damage (Figure 4a) and structural recovery (Figure 4b) of the mineral. The broad features of the signals related to radiation-induced disorder show a characteristic sharpening of their profiles after annealing, especially in the far infrared. The signal in the region around 3400 cm^{-1} indicates the presence of OH species or H_2O in the structure. Temperature-induced spectral changes affect the OH region and absorption decreased in the annealed sample.

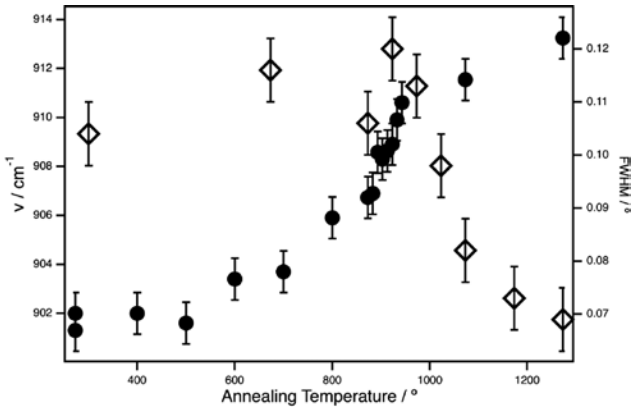

Fig. 7: Thermal evolution of the frequency of the antisymmetric Si–O–Si Raman stretching mode near 902 cm^{-1} (RT) (full circles) and full width at half maximum (FWHM) of the (121) reflection (open squares) of metamict gadolinite-(Y). Estimated error bars are indicated for both data sets.

The unpolarized Raman spectrum of the metamict sample shows broad and weak excitations for the lattice vibrations at lower wavenumbers and stronger intensities near 900 cm^{-1} corresponding to Si–O–Si vibrations of gadolinite-(Y) (Figure 3). The thermal evolution of the frequency of the antisymmetric Si–O–Si Raman stretching mode near 902 cm^{-1} (RT) displayed in Figure 7 shows the onset of recrystallization above 500 K with higher slope between 800 K and ~950 K. A change in slope occurs near 950 K, which might be due to the appearance of another phase.

Using optical spectroscopy in other metamict minerals [5–7, 13, 16, 17] it has been shown that annealing-induced structural recovery of the radiation damaged regions occurs more readily if the sample is not completely damaged [33]. The local, short range structure is seen in Raman spectroscopic investigations where the detectable coherence length of the interatomic vibrations, and hence their structural properties, extends over roughly one molecular complex [34]. Experimentally, our Raman spectra show a rapid critical recrystallization at 943 K. This local effect is only partially mirrored by long range order, as seen by X-ray diffraction. The annealing effects as seen by X-ray diffraction and Raman spectroscopy are shown in Figure 7. The linewidth of the (121) reflection decreases under heating beyond 984 K showing the establishment of an increasingly better ordered crystalline structure while the local order is already established at 943K. The high temperature sharpening of X-ray diffraction profiles is nearly exponential and saturates near 1073 K when a recovered structure is produced.

The metamict gadolinite-(Y) sample in this study shows a Fe^{3+} concentration below the detection limit of the Mössbauer experiment although it is only moderately metamict (amorphous fraction ~18%). This agrees with observations by Malczewski [30] where all samples, regardless of dose, contain only ferrous iron, with the exception of one sample reported to have an oxidised surface. The low level of Fe^{3+} differs from observations in metamict titanite, where Fe^{2+} occurs in the damaged regions combined with Fe^{3+} in the remaining crystalline parts of the metamict mineral [10–12]. In titanite the oxidation of Fe^{2+} to Fe^{3+} therefore mirrors the recrystallization process, which takes place during annealing. In contrast, in gadolinite Fe seems to remain as ferrous iron even during the ballistic metamictization process. In natural titanite, iron was found as Fe^{3+} as well as Fe^{2+} in the octahedral Ti site and in synthetic titanite it was found in approximately equal amounts in octahedral Ti and tetrahedral Si sites [35]. We have no evidence for Fe in Si sites of gadolinite, however, and the octahedral site of Fe in gadolinite is strongly

deformed which does not allow a comparison of the two structures using a simple crystal field approach.

The structural effect of radiation damage was measured and modelled in zircon and showed that high-energy recoils break bonds and cause polymerization, shear deformation, and unit-cell expansion [36]. These authors also demonstrated that the damage depends on the crystal structure, which may also apply to gadolinite. Our study suggests that the structure of annealed, recrystallized gadolinite may deviate slightly from the structure of gadolinite that was never metamict. Further structural investigations are needed to show if the distorted Fe–O-octahedra play a significant role in this context.

Acknowledgements: We thank L. Buiven, S. Heidrich, P. Stutz and J. Ludwig for experimental help and Prof. J. Schlüter for providing the mineral sample from the Mineralogical Museum of the University of Hamburg. EKHS is grateful to EPSRC (EP/PO24904/1) and the Leverhulme Trust (EM-2016-004).

References

[1] R. C. Ewing, The metamict state: 1993 – the centennial. *Nucl. Instrum. Meth. B*, **1994**, *91*, 22.

[2] G. C. Capitani, H. Leroux, J. C. Doukhan, A TEM investigation of natural metamict zircons: structure and recovery of amorphous domains. *Phys. Chem. Miner*. **2000**, *27*, 545.

[3] P. V. Pavlov, N. V. Belov, The crystalline texture of herderite, datolite and gadolinite. *Doklady Akademii Nauk SSSR* **1957**, *114*, 884.

[4] R. Miyawaki, R. Nakai, K. Nagashima, A refinement of the crystal structure of gadolinite. *Am. Mineral*. **1984**, *69*, 948.

[5] T. Beirau, U. Bismayer, B. Mihailova, C. Paulmann, L. A. Groat, Structural phenomena of metamict titanite: a synchrotron, X-ray diffraction and vibrational spectroscopic study. *Phase Trans.* **2010**, *83*, 694.

[6] T. Beirau, B. Mihailova, G. Matveeva, U. Kolb, T. Malcherek, L. A. Groat, U. Bismayer, Structural anisotropy and annealing-induced nanoscale atomic rearrangements in metamict titanite. *Am. Mineral*. **2012**, *97*, 1354.

[7] T. Beirau, B. Mihailova, T. Malcherek, C. Paulmann, U. Bismayer, L. A. Groat, Temperature-induced $P2_1/c$ to $C2/c$ phase transition in partially amorphous (metamict) titanite revealed by Raman spectroscopy. *Can. Min.* **2014**, *52*, 91.

[8] T. Beirau, W. D. Nix, U. Bismayer, L. A. Boatner, S. G. Isaacson, R. C. Ewing, Anisotropic mechanical properties of zircon and the effect of radiation damage. *Phys. Chem. Miner.* **2016**, *43*, 627.

[9] T. Beirau, D. Murawski, H. Behrens, E. K. H. Salje, L. A. Groat, R. Kaden, H. Pöllmann, U. Bismayer, Locally preserved $\alpha \rightarrow \beta$ phase transition in natural radiation-damaged titanite ($CaTiSiO_5$): evidence from laser-induced photoluminescence and dielectric measurements. *J. Phys.: Condens. Matter* **2018**, *30*, 035403.

[10] E. K. H. Salje, D. J. Safarik, J. C. Lashley, L. A. Groat, U. Bismayer, Elastic softening of metamict titanite $CaTiSiO_5$: radiation damage and annealing. *Am. Mineral.* **2011a**, *96*, 1254.

[11] E. K. H. Salje, D. J. Safarik, R. D. Taylor, M. P. Pasternak, K. A. Modic, L. A. Groat, J.C. Lashley, Determination of iron sites and the amount of amorphization in radiation- damaged titanite ($CaTiSiO_3$). *J. Phys.: Condens. Matter* **2011b**, *24*, 052202.

[12] E. K. H. Salje, D. R. Taylor, D. J. Safarik, J. C. Lashley, L. A. Groat, U. Bismayer, R. J. Evans, R. Friedman, Evidence for direct impact damage in metamict titanite $CaTiSiO_3$. *J. Phys.: Condens. Matter* **2012**, *24*, 052202.

[13] P. Zietlow, T. Beirau, B. Mihailova, L. A. Groat, T. Chudy, A. Shelyug, A. Navrotski, R. C. Ewing, J. Schlüter, R. Škoda, U. Bismayer, Thermal annealing of natural, radiation-damaged pyrochlore. *Z. Kristallogr.* **2017**, *232*, 25–38.

[14] R. C. Ewing, A. Meldrum, L. M. Wang, S. X. Wang, Radiation-induced amorphization. in *Transformation Processes in Minerals*, (Ed. P. H. Ribbe) Reviews in Mineralogy & Geochemistry, Vol. 39, Mineralogical Society of America, Washington, DC, p. 319, **2000**.

[15] P. Toledano, U. Bismayer, Phenomenological theory of the crystalline-to-amorphous phase transition during self irradiation. *J. Phys.: Condens. Matter* **2005**, *17*, 6627.

[16] T. Beirau, C. Paulmann, U. Bismayer, Recrystallisation of metamict allanite. *Min. Mag.* **2011**, *75*, 2393.

[17] M. Zhang, E. K. H. Salje, Spectroscopic characterization of metamictization and recrystallization in zircon and titanite. *Phase Trans.* **2003**, *76*, 117.

[18] N. Tomasic, V. Bermanec, A. Gajoic, M. R. Linaric, Metamict minerals: an insight into a relic crystal structure using XRD, Raman spectroscopy, SAED and HREM. *Croat. Chem. Acta* **2008**, *81*, 391.

[19] S. J. Gibson, A.J. Ehlmann, Annealing characteristics of metamict gadolinite from Rode Ranch Texas. *Am. Mineral.* **1970**, *55*, 288.

[20] J. Janeczek, R. K. Eby, Annealing of radiation damage in allanite and gadolinite. *Phys. Chem. Miner.* **1993**, *19*, 343.

[21] K. Hansen, S. Pedersen, H. Fougt, P. Stockmarr, Post Sveconorwegian exhumation and cooling history of the Evje area, southern Setesdal, CentralSouth Norway. *Nor. geol. unders. Bull.* **1996**, *431*, 49.

[22] S. Pedersen, J. Konnerup-Madsen, Geology of the Setesdalen area, South Norway: Implications for the Sveconorwegian evolution of South Norway. *Bull. Geol. Soc. Denmark* **2000**, *46*, 181.

[23] E. Scherer, C. Munker, K. Mezger, Calibration of the lutetium-hafnium clock. *Science* **2001**, *293*, 683.

[24] D. Malczewski, J. E. Frackowiak, E. V. Galuskin, ^{57}Fe Mössbauer spectroscopy and X-ray diffraction study of some complex metamict minerals. *Hyper. Int.* **2005**, *166*, 529.

[25] N. V. Chukanov, S. M. Aksenov, R. K. Rastsvetaeva, R. Kristiansen, I. V. Pekov, D. I. Belakovskiy, K. V. Van, Y. V. Bychkova, S. N. Britvin, Crystal structure of the OH-dominant gadolinite-(Y) analogue $(Y,Ca)_2(Fe,\square)Be_2Si_2O_8(OH,O)_2$ from Heftetjern pegmatite, Norway. *Acta Crystallogr. B* **2017**, *73*, 899.

[26] J. Chrosch, M. Colombo, T. Malcherek, E. K. H. Salje, L. A. Groat, U. Bismayer, Thermal annealing of radiation damaged titanite. *Am. Mineral.* **1998**, *83*, 1083.

[27] S. Rios, E. K. H. Salje, Diffuse X-ray scattering from weakly metamict zircon. *J. Phys.: Condens. Matter* **1999**, *11*, 8947.

[28] G. L. Long, T. E. Cranshaw, G. Longworth, The ideal Mössbauer effect absorber thickness. *Möss. Effect Ref. Data J.* **1983**, *6*, 42.
[29] C. Prescher, C. McCammon, L. Dubrovinsky, MossA: a program for analyzing energy-domain Mössbauer spectra from conventional and synchrotron sources. *J. Appl. Crystallogr.* **2012**, *45*, 329.
[30] D. Malczewski, Fe-57 Mössbauer spectroscopy and X-ray diffraction study of gadolinites REE2Fe2 + Be2Si2O10 from Lower Silesia (Poland) and Ytterby (Sweden). *Nukleonika* **2003**, *48*, 41.
[31] C. A. McCammon, Mössbauer spectroscopy: applications. in *Spectroscopic Methods in Mineralogy*, (Eds. A. Beran and E. Libowitsky) Eötvös University Press, Budapest, 6, p. 369, **2004**.
[32] H. D. Pfannes, U. Gonser, Goldanskii-Karyagin effect versus preferred orientations (texture). *Appl. Phys*. **1973**, *1*, 93.
[33] E. K. H. Salje, J. Chrosch, R. C. Ewing, Is "metamictization" of zircon a phase transition? *Am. Mineral*. **1999**, *84*, 1107.
[34] E. K. H. Salje, Hard mode spectroscopy – experimental studies of structural phase transitions. *Phase Trans*. **1992**, *37*, 83.
[35] I. J. Muir, J. B. Metson, G. M. Bancroft, ^{57}Fe Mössbauer spectra of perovskite and titanite. *Can. Min*. **1984**, *22*, 689.
[36] K. Trachenko, M. Dove, E. K. H. Salje, Structural changes in zircon under a-decay irradiation. *Phys. Rev. B* **2002**, *65*, 180102(R).